Solar and geoneutrinos

L Ludhova [1,2], **M Agostini** [3,4], **K Altenmüller** [4], **S Appel** [4], **V Atroshchenko** [5], **Z Bagdasarian** [1,26], **D Basilico** [6], **G Bellini** [6], **J Benziger** [7], **R Biondi** [8], **D Bravo** [6,27], **B Caccianiga** [6], **F Calaprice** [9], **A Caminata** [10], **P Cavalcante** [11,28], **A Chepurnov** [12], **D D'Angelo** [6], **S Davini** [10], **A Derbin** [13], **A Di Giacinto** [8], **V Di Marcello** [8], **X.F Ding** [9], **A Di Ludovico** [9], **L Di Noto** [10], **I Drachnev** [13], **A Formozov** [14,6], **D Franco** [15], **C Galbiati** [9,16], **C Ghiano** [8], **M Giammarchi** [6], **A Goretti** [9,28], **A.S Göttel** [1,2], **M Gromov** [12,14], **D Guffanti** [17], **Aldo Ianni** [8], **Andrea Ianni** [9], **A Jany** [18], **D Jeschke** [4], **V Kobychev** [19], **G Korga** [20,31], **S Kumaran** [1,2], **M Laubenstein** [8], **E Litvinovich** [5,21], **P Lombardi** [6], **I Lomskaya** [13], **G Lukyanchenko** [5], **L Lukyanchenko** [5], **I Machulin** [5,21], **J Martyn** [17], **E Meroni** [6], **M Meyer** [22], **L Miramonti** [6], **M Misiaszek** [18], **V Muratova** [13], **B Neumair** [4], **M Nieslony** [17], **R Nugmanov** [5,21], **L Oberauer** [4], **V Orekhov** [17], **F Ortica** [23], **M Pallavicini** [10], **L Papp** [4], **L Pelicci** [1,2], **Ö Penek** [1,2], **L Pietrofaccia** [9], **N Pilipenko** [13], **A Pocar** [24], **G Raikov** [5], **M.T Ranalli** [8], **G Ranucci** [6], **A Razeto** [8], **A Re** [6], **M Redchuk** [1,2,30], **A Romani** [23], **N Rossi** [8], **S Schönert** [4], **D Semenov** [13], **G Settanta** [1], **M Skorokhvatov** [5,21], **A Singhal** [1,2], **O Smirnov** [14], **A Sotnikov** [14], **Y Suvorov** [8,5,29], **R Tartaglia** [8], **G Testera** [10], **J Thurn** [22], **E Unzhakov** [13], **F Villante** [8,25], **A Vishneva** [14], **R.B Vogelaar** [11], **F von Feilitzsch** [4], **M Wojcik** [18], **M Wurm** [17], **S Zavatarelli** [10], **K Zuber** [22] **and G Zuzel** [18]

The Borexino Collaboration
[1] Institut für Kernphysik, Forschungszentrum Jülich, 52425 Jülich, Germany
[2] RWTH Aachen University, 52062 Aachen, Germany
[3] Department of Physics and Astronomy, University College London, London, UK
[4] Physik-Department, Technische Universität München, 85748 Garching, Germany
[5] National Research Centre Kurchatov Institute, 123182 Moscow, Russia
[6] Dipartimento di Fisica, Università degli Studi e INFN, 20133 Milano, Italy
[7] Chemical Engineering Department, Princeton University, Princeton, NJ 08544, USA
[8] INFN Laboratori Nazionali del Gran Sasso, 67010 Assergi (AQ), Italy
[9] Physics Department, Princeton University, Princeton, NJ 08544, USA
[10] Dipartimento di Fisica, Università degli Studi e INFN, 16146 Genova, Italy
[11] Physics Department, Virginia Polytechnic Institute and State University, Blacksburg, VA 24061, USA
[12] Lomonosov Moscow State University Skobeltsyn Institute of Nuclear Physics, 119234 Moscow, Russia
[13] St. Petersburg Nuclear Physics Institute NRC Kurchatov Institute, 188350 Gatchina, Russia
[14] Joint Institute for Nuclear Research, 141980 Dubna, Russia
[15] AstroParticule et Cosmologie, Université Paris Diderot, CNRS/IN2P3, CEA/IRFU, Observatoire de Paris, Sorbonne Paris Cité, 75205 Paris Cedex 13, France

[16] Gran Sasso Science Institute, 67100 L'Aquila, Italy

[17] Institute of Physics and Excellence Cluster PRISMA+, Johannes Gutenberg-Universität Mainz, 55099 Mainz, Germany

[18] M Smoluchowski Institute of Physics, Jagiellonian University, 30348 Krakow, Poland

[19] Kiev Institute for Nuclear Research, 03680 Kiev, Ukraine

[20] Department of Physics, Royal Holloway, University of London, Department of Physics, School of Engineering, Physical and Mathematical Sciences, Egham, Surrey, TW20 OEX, UK

[21] National Research Nuclear University MEPhI (Moscow Engineering Physics Institute), 115409 Moscow, Russia

[22] Department of Physics, Technische Universität Dresden, 01062 Dresden, Germany

[23] Dipartimento di Chimica, Biologia e Biotecnologie, Università degli Studi e INFN, 06123 Perugia, Italy

[24] Amherst Center for Fundamental Interactions and Physics Department, University of Massachusetts, Amherst, MA 01003, USA

[25] Dipartimento di Scienze Fisiche e Chimiche, Università dell'Aquila, 67100 L'Aquila, Italy

[26] Present address: University of California, Berkeley, Department of Physics, CA 94720, Berkeley, USA

[27] Present address: Universidad AutÛnoma de Madrid, Ciudad Universitaria de Cantoblanco, 28049 27, Spain

[28] Present address: INFN Laboratori Nazionali del Gran Sasso, 67010 Assergi (AQ), Italy

[29] Present address: Dipartimento di Fisica, Università degli Studi Federico II e INFN, 80126 Napoli, Italy

[30] Present address: Dipartimento di Fisica e Astronomia dellíUniversità di Padova and INFN Sezione di Padova, Padova, Italy

[31] Also at Institute of Nuclear Research (Atomki), H-4001, Debrecen, POB.51., Hungary

E-mail: `l.ludhova@fz-juelich.de`

Abstract. Thanks to the progress of neutrino physics, today we are able of exploiting neutrinos as a tool to study astrophysical objects. The latter in turn serve as unique sources of elusive neutrinos, which fundamental properties are still to be understood. This contribution attempts to summarize the latest results obtained by measuring neutrinos emitted from the Sun and geoneutrinos produced in radioactive decays inside the Earth, with a particular focus on a recent discovery of the CNO-cycle solar neutrinos by Borexino. Comprehensive measurement of the pp-chain solar neutrinos and the first directional detection of sub-MeV solar neutrinos by Borexino, the updated ^{8}B solar neutrino results of Super-Kamiokande, as well as the latest Borexino and KamLAND geoneutrino measurements are also discussed.

Neutrinos interact with matter with a very low probability via weak interactions. This makes their detection challenging. Neutrino detectors must have large volumes, have to be constructed from special radio-pure materials and to be shielded from cosmic rays in underground laboratories. On the other had, thanks to this very same property of small interaction cross sections, neutrinos reach our detectors nearly unperturbed. We can use them as messengers from otherwise unreachable locations inside astronomical objects, as is the solar core or interior of our own planet. Section 1 discusses the comprehensive measurement of the pp chain solar neutrinos [1], recent discovery of the CNO solar neutrinos [2, 3, 4] and the first directional detection of sub-MeV solar neutrinos by Borexino [5, 6, 7, 8], as well as the ^{8}B solar neutrino results of Super-Kamiokande [9, 10]. Section 2 is focused on the latest Borexino [11, 12] and KamLAND [13, 14] geoneutrino results.

1. Solar neutrinos
1.1. Introduction to solar neutrinos
Our Sun is powered by two distinct series of nuclear reactions occurring in the hot solar core, in which Hydrogen is fused to Helium. The pp chain provides about 99% of solar energy.

In the sub-dominant CNO cycle, responsible for the remaining ∼1% of energy, the fusion is catalyzed by the presence of Carbon, Nitrogen, and Oxygen. The relative rates of these processes depend on the temperature. For the stars ∼1.3 times heavier than the Sun, the CNO cycle dominates and thus represents principal mechanism of the stellar Helium creation in the Universe. Solar neutrinos are emitted in both processes, being their only direct probe and prove of existence. Various interactions produce solar neutrinos with distinct energy spectra as it is shown in Fig. 1, where the fluxes are normalized according to the prediction of the Standard Solar Model (SSM) [15]. Several neutrino types are emitted in the *pp* chain, named after the interaction of origin: *pp* neutrinos with the lowest energy spectrum and highest flux, mono-energetic ^{7}Be and *pep* neutrinos, ^{8}B neutrinos, and the only unobserved *hep* neutrinos. The relatively low ^{8}B neutrino flux extends above 10 MeV and it is the only one accessible to the water-based Cherenkov detectors having a few-MeV energy threshold, as Super-Kamiokande. The CNO solar neutrinos are emitted in three distinct interactions, but their spectra are very similar and their weighted sum according to the SSM prediction will be considered in the analysis presented below (Sec. 1.3). Borexino, a liquid scintillator (LS) detector, is the only experiment that succeeded in measuring real-time solar neutrinos with such a low energy threshold to detect all neutrinos species, including the lowest-energy *pp* neutrinos.

Solar neutrinos are emitted in electron flavor. During the propagation, neutrinos undergo flavour transformation, strongly influenced by the dense solar matter (MSW effect [16, 17, 18]) and arrive on the Earth as a mixture of all flavors, with the relative proportions dependent on neutrino energy. Solar neutrinos are detected via the elastic scattering off electrons that is sensitive to all neutrino flavors and has no threshold. The electron flavour has the cross-section about 6 times higher with respect to other flavours and thus the overall measured rate is sensitive to the flavour composition of the incoming flux. The scattered electrons, having a continuous spectrum also when originated by mono-energetic neutrinos, are then causing the emission of either scintillation light in organic liquid scintillators or Cherenkov light in water.

The motivation to measure solar neutrinos continues to be two-fold. We learn about neutrino oscillations, in particular about the matter effects influencing the electron-flavour survival probability for neutrinos passing the dense solar matter or even the Earth during the night. We can also constrain various models of non-standard neutrino interactions [19, 20]. On the other hand, measurements of solar neutrinos are a key to test our understanding of the Sun and stars in general. By comparing neutrino and photon luminosities, we test thermo-dynamical stability of the Sun at the order of 100,000 years, the time needed by electromagnetic radiation to escape from the Sun. The so-called *solar metallicity* problem - the fact that the new low-metallicity inputs to the SSM (LZ-SSM) are spoiling the previous agreement of the SSM using older high metallicity inputs (HZ-SSM) with helio-seismological data. In solar physics, metallicity is the surface abundance of the elements heavier than Helium, that is an input to the SSM influencing predictions of neutrino fluxes. The metallicity influences opacity and thus temperature in the core and the rates of all nuclear reactions. Only for the CNO cycle, this dependence is direct, as C, N, and O are catalyzing this fusion process. The LZ and HZ SSM predictions for the CNO flux differ at about 30% level. Thus, a precise CNO measurement would provide a strong handle on solving this key question of solar physics.

1.2. Borexino latest results on the pp-chain neutrinos

Borexino is the world's radio-purest liquid scintillator detector placed at the Laboratori Nazionali del Gran Sasso in Italy and the only experiment to report a comprehensive measurement of the *pp*-chain solar neutrinos [1]. Analysis of the Phase-II data (December 2011 to May 2016, following an extensive purification campaign) lead to the precision measurement of ^{7}Be neutrinos (2.7%), improved measurement of *pp* neutrinos, and, for the first time, >5σ observation of the *pep* neutrinos. The analysis procedure is based on a multi-variate fit of the energy spectra in the
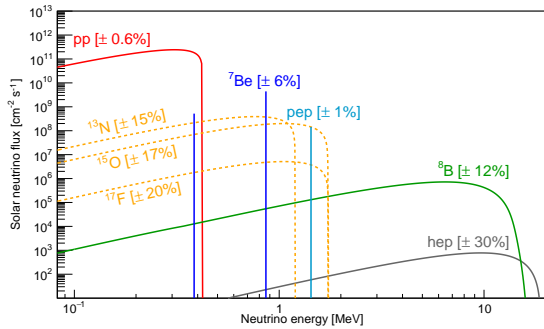
Figure 1. Expected energy spectrum of solar neutrinos from the *pp* chain and CNO cycle nuclear fusion sequences. The flux (vertical scale) is given in units of cm^{-1} s^{-1} MeV^{-1} for continuum sources and in cm^{-1} s^{-1} for mono-energetic sources. From [1] and based on references therein, details in text.

energy range from 0.19 to 2.93 MeV, including pulse-shape and radial distributions of events. The measurement of the ^{8}B neutrino interaction rate above 3.2 MeV of scattered electron is based on the Phase I + II data. By choice, in order not to make any assumptions on its oscillated energy spectrum, ^{8}B analysis is based on radial fits of the selected events. These measurements provide a direct determination of the relative intensity of the two primary terminations of the *pp* chain (*pp*-I and *pp*-II) and an indication that the temperature profile in the Sun is more compatible with the HZ SSM. Assuming SSM predicted solar neutrino fluxes, Borexino determines the electron-flavor survival probability P_{ee} at different energies, thus probing simultaneously the flavor-conversion paradigm both in vacuum- and in matter-dominated regime, excluding the only vaccuum regime at 98.2% C.L.

1.3. Observation of the CNO cycle neutrinos by Borexino

There are several challenges to observe CNO solar neutrinos. Apart its rate being small, the CNO spectral shape is rather feature-less and in addition, highly correlated with that of *pep* solar neutrinos and with the β spectrum of ^{210}Bi, originating in the ^{210}Pb contamination of LS. ^{210}Pb is not a dangerous background by itself, but due to its long-lifetime it is constantly producing ^{210}Bi. Note that the ^{210}Pb is out of equilibrium with the ^{238}U chain, which level of contamination is negligible in Borexino. The *pep* solar neutrino rate can be constrained with 1.4% precision using the solar luminosity constraint and the global fit of solar data excluding the Borexino Phase III data, that were used for the CNO analysis. The main idea to constrain the ^{210}Bi rate is to count on an event-by-event basis the α decays of its daughter, ^{210}Po. This is possible using α/β pulse shape discrimination techniques. Of course, this approach requires a secular equilibrium of the ^{210}Pb-^{210}Bi-^{210}Po chain. Unfortunately, due to the seasonal temperature variations, convective currents have developed in the detector that were bringing additional ^{210}Po from the thin inner nylon vessel (IV), holding the 280 ton of scintillator, to the central 71.3 ton fiducial volume of the analysis. The seasonal variation of the ^{210}Po rate during the Phase II can be seen on the left part of Fig. 2. To minimize the convection, Borexino detector was thermally stabilized by adding a thermal insulation layer and an active temperature control system. Thanks to this, in Phase III a so-called *Low Polonium Field* (LPoF) has developed in the central part of the detector, in which the contribution of convective ^{210}Po is strongly minimized. This is demonstrated by the blue region on the right part of Fig. 2. From a detailed study of the LPoF a minimal value of ^{210}Po has been extracted. This was then considered as an upper limit constraint on ^{210}Bi intrinsic contamination of the LS, since some residual ^{210}Po convection could not be excluded. The LPoF is smaller than the FV of the analysis and thus the level of ^{210}Bi in-homogeneity in the FV was studied. Its level is compatible with the assumption that ^{210}Pb is not de-touching from the IV and only ^{210}Po does. The residual level of ^{210}Bi in-homogeneity was considered as a systematic error on its upper limit constraint. By applying it, together with the *pep* constraint, in the multi-variate fit [4] of the Phase III data (July 2016 - February 2020), the final CNO interaction rate of $7.2^{+3.0}_{-1.7}$ counts per day per 100 ton of LS including all systematic effects, corresponding
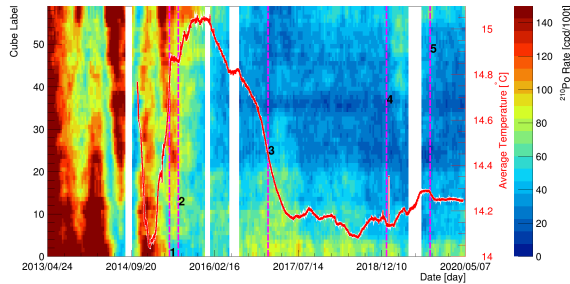
Figure 2. Distribution of $^{210}Po(\alpha)$ events in the Borexino detector in iso-volumes from the bottom to the top of the detector as a function of time (April 2013 - May 2020). Thanks to a thermally stabilized detector in Phase-III, a stable and cleaner region shown in blue has developed. From [2].
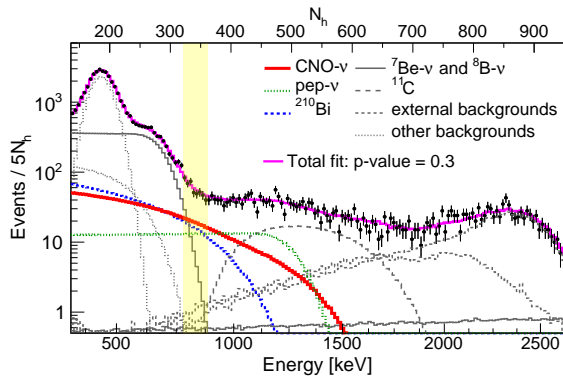

Figure 3. Borexino Phase-III data (black points) and the best fit (magenta) that lead to the first observation of CNO solar neutrinos shown in red. The critical backgrounds are ^{210}Bi internal background (dotted blue) and *pep* solar neutrinos (dotted green), that were constrained in the fit. From [2].

to a CNO flux of $7.0^{+3.0}_{-2.0} \times 10^8\,\mathrm{cm^{-2}\,s^{-1}}$, was extracted. In the multi-variate fit were included two energy spectra, one depleted and one enriched in the cosmogenic ^{11}C background using the Three Fold Coincidence (TFC) technique [21, 22] and a radial distribution of events. The CNO result is compatible with both LZ and HZ SSM. Nevertheless, the existence of the CNO solar neutrinos and occurrence of this fusion in Nature, were confirmed with 5σ at 99% C.L. [2, 4]. This paves the way towards possible future, more precise measurements that could be decisive in solving the solar metallicity puzzle.

1.4. First directional detection of sub-MeV solar neutrinos by Borexino
In LS detectors, the price of high light yield, and thus a possibility of low-energy threshold and a good energy resolution, is paid with the loss of directional information, that is typically present in Water Cherenkov detectors, measuring ^8B solar neutrinos above a few MeV threshold. Borexino has performed [5, 6, 7, 8] the first directionality measurement of sub-MeV solar neutrinos that represents also the first directionality measurement of neutrinos interacting via the elastic scattering off electrons in a LS target. This measurement exploits the sub-dominant Cherenkov light, typically emitted much faster with respect to the slower and dominant scintillation light, to disentangle directional solar neutrino signal from the isotropic background in an energy region around the Compton-like edge of the 0.862 MeV ^7Be solar neutrinos. Using this newly developed *Correlated Integrated Directionality* (CID) method, Borexino measured the ^7Be solar neutrino interaction rate by correlating the PMT positions of the first two hits (after the time-of-flight subtraction) of each selected event with the known position of the Sun, with respect to the reconstructed event vertex. A directional measurement in a classic LS target is an important proof of principle of a possible exploitation of the Cherenkov light in kton-scale next-generation experiments that will use various types of liquid scintillator targets and photo-sensors. Directionality measurement is an important tool for background suppression as well as disentanglement of signals from various directions. In order to achieve more precise

measurements with the CID method, a calibration of the Cherenkov light is fundamental.

1.5. Latest Super-Kamiokande ^8B results

Super-Kamiokande has also provided [10] an update on their ^{8}B solar neutrino measurement [9]. In the SK-IV phase, Super-Kamiokande has improved the removal of cosmogenic radioactive events using neutron captures on Hydrogen and gained 12% exposure, measuring in this phase nearly 64,000 ^{8}B events. By further improving their simulation and reconstruction methods, they achieved a more spatially uniform detector response. Super-Kamiokande updated fit of the solar neutrino oscillation parameters provides a larger Δm_{12}^2 value with respect to the previous analysis, what almost eliminates the previous tension with the KamLAND Δm_{12}^2 result based on reactor antineutrinos. The current agreement of the two Δm_{12}^2 values is at the 1.4σ level and is not influenced by inclusion of the SNO solar data. Super-Kamionkande has studied also the matter effects, both in the core of the Sun (energy dependence of the electron flavour survival probability) and in the Earth (day-night effect). The data favours the MSW spectral distortion at 1.2σ C.L. The observed day-night asymmetry of the ^{8}B solar neutrino flux is $-(0.221 \pm 0.011)$ due to the regeneration of the electron flavour during the night passage through the Earth.

2. Geoneutrinos

2.1. Introduction to geoneutrinos

Geoneutrinos are electron-flavor anti-neutrinos emitted in the β decays of long-lived radioactive elements, the *heat producing elements* (HPE) ^{238}U, ^{232}Th, and ^{40}K. The main aim of geoneutrino studies is to determine the Earth's radiogenic heat. The latter, together with the residual heat from the times of the Earth's accretion, are expected to be the the main contributions to the Earth's heat budget. Geoneutrinos are a unique new tool to study the deep mantle and in particular, its radiogenic heat: a critical parameter in understanding of our planet. Provided the abundances of HPE are known, the radiogenic heat is directly determined via the known nuclear physics. The geoneutrino studies are, however, complicated through an unknown distribution of HPE, on which depends both the geoneutrino signal prediction as well as the final interpretation of the measured geoneutrino flux. The Neutrino Geoscience is thus an excellent example of a new and truly inter-disciplinary field. The HPE are due to their chemical affinity concentrated in the Earth's crust, that is relatively well known thanks to the possibility of direct sampling. In order to estimate the expected mantle geoneutrino signal, one has to rely on the so-called Bulk Silicate Earth Models (BSE). They predict the average composition of the primitive Earth, that roughly corresponds to the remixed present-day mantle and crust. Thus, by subtracting the "known" crustal contribution, one obtains the expected HPE abundances in the mantle. The BSE models can be then compared with the geoneutrino measurements, assuming various scenarios of HPE distribution.

Geoneutrinos are detected via the inverse-beta decay (IBD) reaction $\bar{\nu}_e + p \rightarrow e^+ + n$, a charge-current interaction sensitive only to electron flavor neutrinos. Organic LS are used as proton-rich targets. Only antineutrinos with energies above $1.8\,\text{MeV}$, the IBD kinematic threshold, can be detected: leaving ^{40}K geoneutrinos unreachable to present day detection techniques. Reactor neutrinos are detected by the very same process and represent an irreducible background in geoneutrino measurements. The IBD interaction provides, however, a powerful tool to suppress other types of backgrounds, thanks to a possibility to require a space and time coincidence between the prompt and delayed signals. The positron comes quickly to rest and then annihilates emitting two $511\,\text{keV}$ γ-rays, yielding a *prompt event*. The visible energy E_{prompt} is directly correlated with the incident antineutrino energy $E_{\bar{\nu}_e}$: $E_{prompt} = E_{\bar{\nu}_e} - 0.784\,\text{MeV}$. The neutron, also produced in the IBD, is typically captured on a proton with $\tau = 200$ - $250\,\mu\text{s}$, depending on the scintillator. The capture is followed by a $2.22\,\text{MeV}$ de-excitation γ-ray providing a coincident *delayed event*. Geoneutrino signal is often expressed in *Terrestrial Neutrino Units* (TNU), i.e.
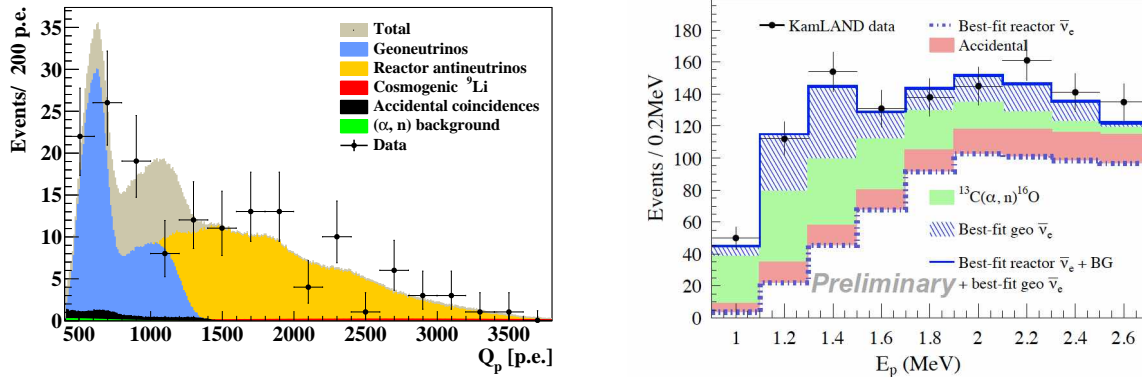
Figure 4. Latest geoneutrino measurements, e.g. energy spectra of the prompt IBD candidate with the best fit, from the Borexino [11] (left) and KamLAND [14] (right) experiments.

1 antineutrino event detected via IBD over 1 year by a detector with 100% detection efficiency containing 10^{32} free target protons (roughly corresponds to 1 kton of a typical LS).

2.2. Borexino and KamLAND latest results

Today, only two experiments succeeded to measure geoneutrinos: Borexino at the LNGS laboratory in Italy and KamLAND in the Kamioka mine in Japan, with the respective latest fits of the energy spectra of the prompt IBD candidates shown in Fig. 4.

Borexino latest result [11, 12] is based on the analysis of 154 IBD candidates and the exposure of $(1.12 \pm 0.05) \times 10^{32}$ protons $\times$ yr acquired between December 2007 and April 2019. Based on the unbinned likelihood fit with the contributions from geoneutrinos and reactor antineutrinos left free, the geoneutrino signal was extracted. It corresponds to $52.6^{+9.4}_{-8.6}$ (stat)$^{+2.7}_{-2.1}$ (sys) geoneutrinos from ^{238}U and ^{232}Th, what corresponds to a geoneutrino signal of $47.0^{+8.4}_{-7.7}$ (stat)$^{+2.4}_{-1.9}$ (sys) TNU, e.q. a signal with $^{+18.3}_{-17.2}$% total precision. The non-antineutrino backgrounds, dominated by accidental coincidences, decays of cosmogenic ^{9}Li, and (α, n) reactions on ^{13}C triggered by ^{210}Po decays, were constrained in the fit according to the expectations (total of about 8 events). The mantle contribution, extracted by constraining the contribution from the bulk lithosphere according to the expectation based on a detailed geological study [23] of the area around LNGS, corresponds to $28.8^{+5.5}_{-4.6}$ events. The resulting mantle signal is $21.2^{+9.6}_{-9.0}$ (stat)$^{+1.1}_{-0.9}$ (sys) TNU and its null-hypothesis is excluded at a 99% C.L. The mantle signal corresponds to the production of a radiogenic heat of $24.6^{+11.1}_{-10.4}$ TW (68% interval) from ^{238}U and ^{232}Th in the mantle. Even though Borexino results are compatible with different BSE models, there is a $\sim 2.4\sigma$ tension with those predicting the lowest HPE concentrations.

The latest geoneutrino result published by KamLAND [13] in 2013 was followed by a preliminary update presented [14] at the Neutrino Geoscience conference in 2019 and includes the low-reactor background data until April 2018. The whole data set of 7.2×10^{32} target-proton $\times$ year exposure includes the three different periods: Period 1 (2002-2007) before the LS purification with large amount of reactor, accidental, and (α, n) backgrounds; Period 2 (2009-2011) after the purification, with the non-antineutrino background strongly suppressed, and Period 3, after the 2011 Fukushima accident, with a strong reduction of reactor antineutrino background. The fit of 1167 prompt IBD candidates includes the rate, shape, and time analysis. It yielded $168^{+26.3}_{-26.5}$ geoneutrinos, what corresponds to a geoneutrino signal of $32.1^{+5.0}_{-5.0}$ TNU, e.q. a signal with $^{+15.6}_{-15.7}$% total precision. The mantle contribution is obtained by a subtraction of the crustal one based on [24]. This leads to a mantle signal of of $6.0^{+5.6}_{-5.7}$ TNU and radiogenic heat

of about 5.4 TW from ^{238}U and ^{232}Th in the mantle. KamLAND thus prefers the BSE models with the lowest or intermediate HPE abundances.

2.3. Summary and outlook

In this contribution were discussed the latest solar and geoneutrino results. Borexino has performed a complete spectroscopy of the *pp* chain solar neutrinos and observed the CNO cycle solar neutrinos. This achievement paves the way for the future experiments to eventually solve the metallicity problem of the present-day solar physics. In addition, Borexino has performed the first directional detection of sub-MeV solar neutrinos. Borexino has stopped data taking in October 2021, but will continue to analyse the latest data with the best thermal stability of the detector, that might lead to an improved CNO measurement. Super-Kamiokande has improved the analysis of the SK-IV phase ^{8}B solar neutrino data and updated the oscillation analysis. The previous tension with KamLAND reactor data about the Δm^2_{12} mass splitting is now resolved. The MSW spectral distortion due to the matter effects in the Sun is slightly favoured. Borexino and KamLAND have observed geoneutrinos with a high statistical significance. Their results are in some tension when homogeneous mantle is assumed, but both are consistent with the range of different BSE models. The next generation of experiments are needed to provide results leading to firm geological conclusions. The SNO+ [25, 26] LS experiment in Canada is expected to provide the geoneutrino and solar neutrino results in the near future. JUNO [27, 28], the 20 kton LS detector under construction in China, has a huge potential in both fields. The ultimate geoneutrino measurement could be achieved with an Ocean Bottom Detector [29], in which the mantle signal would dominate the total geoneutrino signal.

References

[1] Agostini M et al. (Borexino Collaboration) 2018 *Nature* **562** 496
[2] Agostini M et al. (Borexino Collaboration) 2020 *Nature* **587** 577
[3] Penek Ö et al. (Borexino Collaboration) parallel talk 35 and proceedings of TAUP 2021
[4] Pellici L et al. (Borexino Collaboration) poster 263 and proceedings of TAUP 2021
[5] Agostini M et al. (Borexino Collaboration) 2020 arXiv:2109.04770 and submitted to PRD
[6] Martyn J et al. (Borexino Collaboration) parallel talk 267 and proceedings of TAUP 2021
[7] Singhal A et al. (Borexino Collaboration) poster 270 and proceedings of TAUP 2021
[8] Kumaran S et al. (Borexino Collaboration) poster 220 and proceedings of TAUP 2021
[9] Abe K et al. (Super-Kamiokande Collaboration) 2016 *Phys. Rev. D* **94** 052010
[10] Smy M et al. (Super-Kamiokande Collaboration) 2021 *Private communication*
[11] Agostini M et al. (Borexino Collaboration) 2020 *PRD* **101** 012009
[12] Kumaran S et al. (Borexino Collaboration) parallel talk 221 and proceedings of TAUP 2021
[13] Gando A et al. (KamLAND Collaboration) 2013 *PRD* **88** 033001
[14] Watanabe H et al. (KamLAND Collaboration) talk at the Neutrino Geoscience Conference, October 21-23, 2019, Prague, Czech Republic
[15] Vinyoles N et al. 2017 *Astrop. Phys. J* **835** 202
[16] Pontecorvo B 1967 *Zh. Eksp. Teor. Fiz.* **53** 1717
[17] Wolfenstein L 1978 *Phys. Rev. D* **17** 2369
[18] Mikheyev S and Smirnov A 1985 *Sov. J. Nucl. Phys.* **42** 913
[19] Minakata Y and Peña-Garay C 2012 *Adv. High En. Phys.* **2102** ID 349686
[20] Agarwalla S K et al. (Borexino Collaboration) 2020 *JHEP* **2020** 38
[21] Agostini M et al. (Borexino Collaboration) 2020 arXiv:2106.10973 and submitted to EPJC
[22] Porcelli A et al. (Borexino Collaboration) poster 477 and proceedings of TAUP 2021
[23] Coltorti M et al. 2011 *Geochim. Cosmoch. Acta* **75** 2271
[24] Enomoto S et al. 2007 *EPSL* **258** 147
[25] Albanese V et al (SNO+ Collaboration) 2021 *JINST* **16** P08059
[26] Chen M et al. (SNO+ Collaboration) parallel talk 396 and proceedings of TAUP 2021
[27] An F et al. (JUNO Collaboration) 2016 *J. Phys.* **G43** 030401
[28] Settanta G et al. (JUNO Collaboration) parallel talk 273 and proceedings of TAUP 2021
[29] SAKAI T et al. (OBD working group) parallel talk 197 and proceedings of TAUP 2021